Propagating spin waves excited by spin-transfer torque: a combined electrical and optical study

M. Madami,[a] E. Iacocca,[b,c] S. Sani,[d] G. Gubbiotti,[e] S. Tacchi,[e] R.K. Dumas,[b] J. Åkerman,[b,d] and G. Carlotti[a]

[a]   Physics Department, University of Perugia, Perugia, Italy
[b]   Physics Department, University of Gothenburg, Gothenburg, Sweden
[c]   Department of Applied Physics, Division for CMT, Chalmers University of Technology, Gothenburg, Sweden
[d]   Materials Physics, School of ICT, Royal Institute of Technology (KTH), Kista, Sweden
[e]   Istituto Officina dei Materiali del Consiglio Nazionale delle Ricerche (IOM-CNR), Unità di Perugia c/o Dipartimento di Fisica, Perugia, Italy

Abstract

Nanocontact spin-torque oscillators are devices in which the generation of propagating spin waves can be sustained by spin transfer torque. In the present work, we perform combined electrical and optical measurements in a single experimental setup to systematically investigate the excitation of spin waves by a nanocontact spin-torque oscillator and their propagation in a $Ni_{80}Fe_{20}$ extended layer. By using microfocused Brillouin light scattering we observe an anisotropic emission of spin waves, due to the broken symmetry imposed by the inhomogeneous Oersted field generated by the injected current. In particular, spin waves propagate on the side of the nanocontact where the Oersted field and the in-plane component of the applied magnetic field are antiparallel, while propagation is inhibited on the opposite side. Moreover, propagating spin waves are efficiently excited only in a limited frequency range corresponding to wavevectors inversely proportional to the size of the nanocontact. This frequency range obeys the dispersion relation for exchange-dominated spin waves in the far field, as confirmed by micromagnetic simulations of similar devices. The present results have direct consequences for spin wave based applications, such as synchronization, computation, and magnonics.

I. Introduction

Nanocontact (NC) based spin-torque oscillators (STOs) [1] have been extensively studied in recent years due to their potential applications in a variety of fields including, spintronics, magnonics, [2] and data storage [3]. NC-STOs typically consist of an extended pseudo-spin-valve where two magnetic layers are separated by a nonmagnetic spacer. One of the magnetic layers is a hard magnet that acts as spin polarizer and a reference layer, and it is referred to as the "fixed" layer. The second, "free" magnetic layer is softer and thinner, making it susceptible to spin-transfer torque (STT) induced dynamics [4, 5]. Depending on the material used for the free layer, unique magnetodynamical modes can be generated in NC-STOs. On the one hand, by using Co/Ni multilayers exhibiting perpendicular magnetic anisotropy, NC-STOs have been shown to support steady magnetization dynamics at low external fields [6] and even the excitation of localized modes known as magnetic dissipative droplets [7, 8, 9, 10]. On the other hand, using soft magnets such as NiFe, the existence of propagating [11, 12], localized [12, 13, 14, 15], and vortex [16, 17] modes has been demonstrated, depending on both the strength and the direction of the external magnetic field.

The propagating mode was first predicted theoretically by Slonczewski [18] for a perpendicularly magnetized NC-STO, *i.e.* by applying an external magnetic field perpendicular to the device normal strong enough to saturate the free layer. This mode has been shown to consist of exchange-dominated spin waves (SWs) propagating radially away from the NC region at frequencies above the ferromagnetic resonance (FMR) frequency and with a wavenumber inversely proportional to the NC diameter. The propagating nature of this mode lends itself to coupling NC-STOs to achieve better spectral features by synchronization [19, 20, 21, 22, 23], to perform computation [24, 25], or to propagate information in magnonic devices [26, 27].

The existence of the propagating mode was demonstrated only recently, by employing either electrical measurements [28], to study SW-mediated synchronization, or microfocused Brillouin light scattering (μ-BLS) [11] to directly detect the emitted SWs. Although these experiments provided unambiguous proof of the propagating character of this mode, micromagnetic simulations including the Oersted field generated by the bias current [13, 29] predicted that the propagation is generally anisotropic, especially if the applied field is tilted away from the device normal. This has tremendous consequences for the design and application of devices utilizing STT-driven SWs. However, to the best of our knowledge, no *direct* experimental evidence of such asymmetric propagation has been provided to date for out-of-plane magnetized NC-STOs. Evidence of asymmetric emission has been experimentally demonstrated only for in-plane magnetized NC-STOs by the works of Demidov at al. [15, 30]

In the present work, we combine electrical characterization and μ-BLS in a single experimental setup to systematically investigate both the electrical properties of the STT-induced dynamics and the characteristics of the propagating SWs excited in an out-of-plane magnetized NC-STO. Evidence is provided for anisotropic

SW propagation in these devices, as reproduced by micromagnetic simulations. More importantly, the STT-generated SWs are found to propagate within a wavevector range dictated by both the SW dispersion in the far-field and the diameter of the NC. In fact, micromagnetic simulations reveal that nonlinear dynamics are strongly damped close to the NC (near-field region), while only wavevectors obeying the SW dispersion relation are able to propagate in the far-field region, i.e. at distances longer than the NC dimensions. These results are relevant for the development of SW-based devices, including the synchronization of NC-STO arrays, computation, and magnonics.

II. Experimental Details

Samples were fabricated on a SiO_2 (1 µm) covered silicon wafer through the following processing steps: a pseudo-spin-valve stack of Pd (8 nm) / Cu (15 nm) / Co (8 nm) / Cu (8 nm) / $Ni_{80}Fe_{20}$ (4.5 nm) / Cu (3 nm) / Pd (3 nm) was deposited by magnetron sputtering then, making use of photolithography, rectangular 8×16 µm^2 mesas were defined. A 30 nm thick SiO_2 layer was deposited on top of the mesas to realize electric insulation of the devices. 2×4-µm^2 ground electrodes and circular NCs with 100-nm diameter were then defined in this insulation layer above each mesa. Finally, contact pads with ground–signal–ground (GSG) geometry, as depicted in Fig. 1(c), were fabricated with sputter deposition of 1 µm Cu / 20 nm Au in a photolithography prepared lift-off pattern. The final device allows for μ-BLS optical access on one side of the NC only, as shown in Fig.1(c).

Measurements in the frequency domain were performed using a broadband spectrum analyzer (SA). A DC was injected into the NC while the device impedance was continuously monitored in order to avoid damage due to Joule heating. The direction of the injected DC is negative (*i.e.* electrons drift from the free to the fixed layer) as required to obtain an STT-induced enhancement of the magnetization dynamics in the free layer [11]. Notably, this approach is only sensitive to the magnetodynamics generated very near the NC, along the path of the DC current.

μ-BLS measurements were performed applying an external magnetic field H at an angle of about 15° from the sample normal, by means of a customized projected field electromagnet. As has already been demonstrated in a previous paper [11], the out-of-plane magnetized NC geometry favors the emission of propagating SWs in the extended portion of the NiFe free layer. At the same time, the slight tilt of the external field allows us to define the direction of the in-plane component of the field, H_{IP}, as shown in Fig.1. This choice is crucial in defining the direction of the propagating SWs, as we will demonstrate below. The emitted SWs were experimentally detected at room temperature by means of a μ-BLS setup described in detail elsewhere [31]. We measured the Stokes side of each spectrum only, in order to halve the total acquisition time. This approach is justified by the symmetry of the Stokes and anti-Stokes sides of the spectrum in a measurement performed at normal incidence in a thin magnetic film [33].

To summarize, our setup allows us to electrically investigate the generated dynamics of the NC-STO while simultaneously characterizing the emitted SWs by μ-BLS.

III.   Micromagnetic simulations

Micromagnetic simulations were performed using the graphic processing unit (GPU) accelerated software Mumax3 [34]. The extended free layer was modeled by a disk with a diameter of 2.2 μm and absorbing boundary conditions (ABC) to prevent spurious generation and reflection of SWs. The ABCs were implemented by linearly increasing the Gilbert damping coefficient over 200 nm towards the disk edge, so that the active area of the model was a 1.8 μm diameter disk. We considered the device nominal free layer thickness to be 4.5 nm and the magnetic parameters as follows: saturation magnetization $\mu_o M_S = 0.69$ T, Gilbert damping $\alpha = 0.01$, exchange stiffness $A = 11$ pJ/m, and no magnetocrystalline anisotropy. These parameters define the cell discretization to $4.3 \times 4.3 \times 4.5$ nm, below the exchange length $\lambda_{ex} \approx 6$ nm, resulting in a 512×512 mesh. STT was considered only in a cylindrical region defined by the NC of diameter $d = 100$ nm positioned in the geometrical center of the disk. We assumed a polarization consistent with a Co layer, $P = 0.3$, and a symmetric torque $\lambda = 1$, as has previously been shown to model similar devices with high accuracy [13, 14]. The direction of the fixed layer was calculated numerically by solving the magnetostatic boundary conditions for a Co thin film with saturation magnetization $\mu_o M_P = 1.5$ T. Both the external applied field and the current-generated Oersted field were included in the simulations. Unless specified, the simulations were performed with a fixed time step of 10 fs and at room temperature.

The spectral characteristics of the generated dynamics can be estimated from 10 ns long simulations sampled at 10 ps, returning a frequency resolution of ≈ 97 MHz. Field-dependent simulations indicate that high field magnitudes are required to excite well-defined SWs. This can be understood from the fact that demagnetizing fields arise at the boundaries of the simulated disk, favoring a vortex ground state. Applied fields of magnitude $\mu_o H > 650$ mT are numerically found to preclude the formation of a vortex and to allow the excitation of STT-induced propagating SWs.

IV.   Results and discussion

- *Anisotropic spin-wave emission and decay length*

The first step of our experiment was to investigate the effect of varying the direction of the in-plane component of the external magnetic field (H_{IP}) on the spatial distribution of SWs emitted below the NC area. To perform such an experiment the external field intensity was set to $\mu_o H = +700$ mT and the field direction was tilted so that its in-plane component was antiparallel to the Oersted field on the side of the NC which is accessible to μ-BLS, as shown in Fig.1(a). By injecting a DC of $I = 30$ mA into the NC, we were able to

obtain steady-state oscillations at a frequency of 15.5 GHz and with an intensity of about +9 dB over noise, as measured by the SA. In order to map the intensity of the emitted SWs, we then performed a two-dimensional μ-BLS scan over an area of about 2×1 μm^2 on the optically accessible NC side and at a distance of about 1 μm from the NC itself. The measured two dimensional map, shown in Fig. 1(a), was obtained by integrating the measured SW intensity in a frequency range of 0.5 GHz around the central value of 15.5 GHz. This μ-BLS map clearly shows emission from the NC area, confined in a relatively narrow beam which propagates in the direction perpendicular to both the direction of the Oersted field and H_{IP}. If the external field polarity is reversed ($\mu_o H$ = -700 mT), the Oersted field and H_{IP} become parallel on the optically accessible NC side, [35] but no SWs are detected in this case, as shown by the μ-BLS map in Fig. 1b.[1] This clearly demonstrates anisotropic spin-wave emission, confirming previous numerical predictions indicating that the largest SW intensity is emitted on the side of the NC where the Oersted and the H_{IP} fields are antiparallel [13, 29]. As the second step of this investigation, we measured the decay of the emitted SW intensity (i) as a function of the distance from the NC position (X-X_0), by scanning the laser probe along the X-direction. The results of these measurements are shown in Fig. 2 (black dots) together with the result of a best fit analysis obtained using the following analytical expression:

$$i(X) = i_0 + \frac{A}{X-X_0} \cdot e^{-\frac{X-X_0}{l}}$$ (1)

where i_0 is the baseline, X_0 is the NC position (fixed at $X_0 = 0$), and l is the decay length of SW intensity; A and l are the free parameters in the fit routine, which returns a value of $l = 500 \pm 50$ nm. This is in very good agreement with the expected value obtained from the expression $l = v_g/2\alpha\omega = 500$ nm, where $v_g = 1.0$ μm/ns is the SW group velocity extracted from the simulated dispersion curve of the free layer (see Fig. 5), $\alpha = 0.01$ is the conventional value of damping in NiFe, and $\omega = 2\pi f$ is the SW angular frequency ($f = 15.5$ GHz).

- *Dependence of the spin-wave emission on the injected current and applied field intensity*

Next, we turn our attention to the characteristics of the emitted SWs by simultaneously measuring the spectra obtained electrically and optically when varying either the intensity of the external magnetic field H or the direct current I. The results reported in Fig. 3 were obtained by injecting a constant current $I = 30$ mA and applying an external magnetic field of variable intensity (in the range H = 550–800 mT) with its in-plane component (H_{IP}) directed as in Fig. 1(a), to favor the emission of SWs on the optically accessible side of the device. The first two panels show the μ-BLS spectra of SW intensity measured at a fixed position of about 1.0 μm away from the NC, Fig. 3(a), and the sequence of spectra acquired with the SA, Fig. 3(b) as a function of H. The same data are reported in Fig. 3c and Fig. 3d on color-scale bidimensional plots. The data

---

[1] The frequency of the steady-state oscillations as measured by the SA only changed by a small amount (from 15.5 to 15.3 GHz) when the applied field was reversed, while its intensity increased to +10 dB over noise.

obtained from μ-BLS features two well-defined peaks. The lowest frequency peak, which is not observed on the SA spectra, Fig. 3(d), exhibits a constant intensity and can be measured even for $I = 0$, *c.f.* red spectrum in Fig. 4(a). It corresponds to the thermally activated FMR mode of the NiFe layer, consistent with Kittel's equation as a function of **H**. The highest frequency peak of Fig. 3(c) is instead observed in the SA spectra at the same frequency for all the measured fields and corresponds to the SWs emitted by the STT-driven precession of the magnetization under the NC. The blue-shift of this peak with respect to the FMR frequency is a signature of the propagating character of the SWs emitted away from the NC which is further confirmed by the fact that its signal is measurable up to about 2.2 µm away from the NC itself, as was shown in Fig. 2. The positive field tunability of this mode is estimated to be 24 MHz/mT. A comparison of the above experimental results with those obtained from micromagnetic simulations, Fig. 3(e), accounts for a very good quantitative agreement over the entire range of fields we investigated. Careful inspection of the measured spectra reveals the presence of a mode transition for a field value of **H** = 675 mT, denoted by two resonant frequencies in both the μ-BLS and SA spectra. Corresponding to this mode transition, the SA spectrum is strongly modified, exhibiting a shaper and stronger peak. The occurrence of such mode transitions is very common in this kind of NC-STO devices [28] and reflects the complicated nonlinear dynamics that can also be affected by unique and local features of the real NC. As a matter of fact, nominally identical devices present one or more mode transitions at different field/current values, or even no transitions at all.

A direct comparison of the measured peaks corresponding to the FMR and STT modes in the μ-BLS spectra, Fig. 3(a), suggests that the two modes have comparable intensities. This result may seem surprising at first, since a much larger intensity should be expected for STT-driven SWs than for thermally excited SWs. The reason for this apparent inconsistency lies in the wavevector content of the two modes and how it is efficiently collected by the optics of our experimental setup. By combining the effect of the finite collection angle ($\theta = 48.6°$, NA = $\sin(\theta) = 0.75$) of our microscope objective with the effect of the uncertainty in the in-plane component of the wavevector of the scattered photons, resulting from the limited spatial extent of the laser spot on the sample ($\approx$ 300 nm), it is possible to demonstrate that the efficiency of our apparatus in detecting SWs with small wavelengths decreases very rapidly as the wavelength is reduced below 300 nm [11]. Since the diameter of the NC under investigation is only 100 nm, we expect the wavelength of propagating SWs to be smaller than 200 nm [18], which means we can detect them with relatively low efficiency in our apparatus.

Figure 4 shows the results of a second set of simultaneous μ-BLS and SA characterizations obtained by setting the external field intensity to a fixed value of **H** = 680 mT and varying the intensity of the injected DC (*I*) over the range between 23.0 and 38.0 mA. The first μ-BLS spectrum (red line) in Fig. 4(a) was measured at $I = 0$ mA, showing the thermal FMR mode. In the following sequence of μ-BLS spectra, Fig. 4(a), the FMR signal was no longer acquired, in order to reduce the acquisition time and because its frequency does not vary with current, so the only visible peak in the spectra is the one corresponding to the STT-driven SW excitation. Fig. 4(b) shows the corresponding sequence of SA spectra, while Fig. 4(c) and

Fig. 4(d) report the same μ-BLS and SA measurements in bidimensional color scale plots. Similarly as in the case of the field characterization (Fig. 3), we observed a blue-shift of the STT-driven SW frequencies with respect to the FMR, as well as a positive current tunability that we estimate to be 250 MHz/mA. On increasing I, a mode transition is observed for the value of $I = 29.0$ mA; this is characterized by a relatively large frequency jump of about 2 GHz, clearly visible in the SA sequence of spectra, and accompanied by a dramatic reduction in linewidth and an increase in maximum intensity. It is interesting to note how the signal coming from propagating SWs, as measured by μ-BLS, is easily detectable only over a finite range of currents, $I = 29.0 – 35.0$ mA, after the mode transition. Before the mode transition ($I < 29.0$ mA) the SW signal is hardly detectable, probably because of the very low STT efficiency, as is confirmed by the electric measurements. More interesting is the existence of an upper bound ($I = 35.0$ mA) above which the intensity of the emitted SWs rapidly decreases. This is discussed in greater detail in the following.

The existence of a well-defined DC range (and a corresponding frequency range), in which propagating SWs are experimentally detected, is a reproducible feature that we observed in several NC-STO devices with slightly different NC diameters, in the range 80-120 nm, obtaining results which are in good qualitative agreement with those presented in this paper. In order to shed more light on this effect we calculated the dispersion curve for SWs in the out-of-plane magnetized NiFe layer ($H = 680$ mT). The resulting frequency vs. $1/\lambda$ plot is shown in Fig. 5(b), where it is compared with the frequency vs. I plot of Fig. 5(a). We can see good quantitative agreement between the frequency of the FMR mode, as measured by μ-BLS, and the simulated frequency at $1/\lambda = 0$ ($k = 2\pi/\lambda = 0$). From a direct comparison between the two panels in Fig. 5, it is clear that the finite frequency range detected experimentally, corresponds to a finite wavelength range of $\lambda = 115–150$ nm. This is the central result of the present work as it suggests that propagating SWs emitted by an out-of-plane magnetized NC-STO have a limited range of accessible wavelengths, which is ultimately associated with the NC diameter and the exchange-dominated dispersion relation of SWs. In other words, a NC-STO cannot efficiently excite exchange-dominated SWs with a wavelength much shorter (or longer) than its own NC diameter. This has tremendous implications for the synchronization of NC-STOs, since the wavelength unambiguously determines the phase difference between the devices and ultimately the phase-locking condition.

The above observations can be further tested using micromagnetic simulations. Due to the finite size of the simulated disk, much stronger fields are required to obtain a coherent SW emission. Consequently, we set a field of magnitude $H = 800$ mT tilted 15° from the plane normal in the following simulations. To characterize the allowed propagating SWs, we performed simulations at T = 0 K and determined their wavelength as a function of distance via smoothed pseudo-Wigner-Ville (SPWV) transform. By this method, it is possible to tune the real and reciprocal space resolution by making use of smoothing windows. The wavelength content of the generated SW is determined by performing a SPWV transform on a simulation snapshot along the X direction, where we used a Gaussian window of 4.3 nm for the real space and a Hann window of 1.9 μm^{-1} for the reciprocal space. We then averaged 100 SPWV transforms, each one calculated

from different snapshots of the same time-dependent simulation, to further improve the accuracy of the method. The results for NC-STO driven at 34 mA and 25 mA are shown as color plots in Fig. 6(a) and (b), respectively, where the vertical black lines indicate the boundaries of the NC and the color represents the normalized SW magnitude in logarithmic scale. The choice of the values for I was made in order to have one value below the SW emission threshold (25 mA) and the other one right in the middle of that range (34 mA), as confirmed by Fig.5(a). We remind the reader that this figure must be understood as the wavelength content (y axis) as a function of distance for the SW propagating along X. Whether the NC-STO is driven at 34 mA, Fig. 6(a), or 25 mA, Fig. 6(b), most of the wavelength content is rapidly damped within about 0.2 μm from the NC center (near-field region). This strong wavelength content describes the nonlinear forced dynamics of the system due to the presence of strong/local effects in the NC area such as the STT effect and the Oe-field. However, when the NC is driven at 34 mA, Fig. 6(a), a band of wavelengths is observed to prevail up to the simulation boundary, and only in the +X direction. This wavelength band is in good quantitative agreement with the wavelength analytically obtained from the SW dispersion relation for NiFe at the driven NC-STO frequency (white dashed line) and similar to the NC diameter. In contrast, when the NC-STO is driven at 25 mA, Fig. 6(b), this wavelength band, although present, is rapidly damped within about 0.6 μm, corresponding to a scenario in which the Oersted field strongly distorts the magnetic landscape. It is worth mentioning that these results indicate that SW do propagate in the -X direction as well, as expected from exchange-coupling, but their energy is negligible for distances greater than 0.5 μm from the NC. An additional interesting feature of Fig. 6 is that the wavelengths close to the NC boundary are lower (higher) in the +X (-X) direction corresponding to the decrease (increase) of the local field magnitude induced by the Oersted field.

V. Conclusions

The properties of propagating spin waves emitted by an out-of-plane magnetized NC-STO were investigated by means of a combined RF and microfocused BLS experimental setup. We experimentally demonstrated the anisotropic emission of spin waves which is concentrated on the side of the NC where the Oersted field and the in-plane component of the external field are antiparallel. The analysis of both the field and the current tunability of the device showed a clear blue-shift of the STT-excited SW frequency with respect to the FMR one, as well as the presence of abrupt mode transitions. More importantly, it was found that propagating spin waves are only efficiently excited over a limited interval of wavelengths comparable with the NC diameter. Given the dispersion relation in the far-field, this corresponds to a range of frequencies of a few GHz. We believe these results will be of the utmost importance for further progress in NC-STOs synchronization, computation, and magnonic applications via emitted spin waves.

Acknowledgements
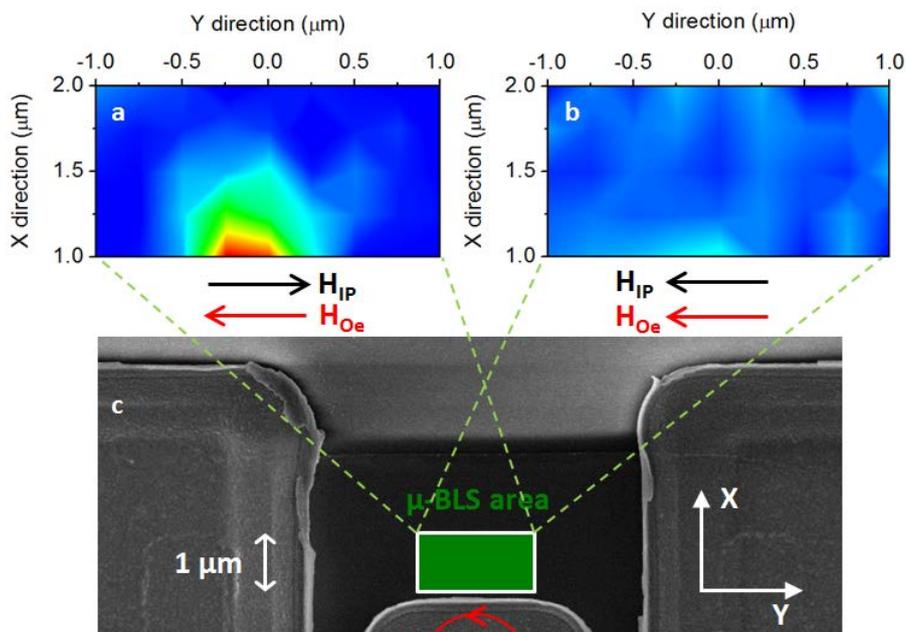
Figure 1 (color online). (a) and (b): Spin-wave intensity maps measured by μ-BLS in the green area of panel (c), for two different directions of the in-plane component (H_{IP}) of the external field, $\boldsymbol{H} = 700$ mT and $I = 30$ mA. (c) SEM image of the device with the ground-signal-ground (GSG) pads, NC position and the direction of the Oe field generated by the current (I) flowing into the NC.
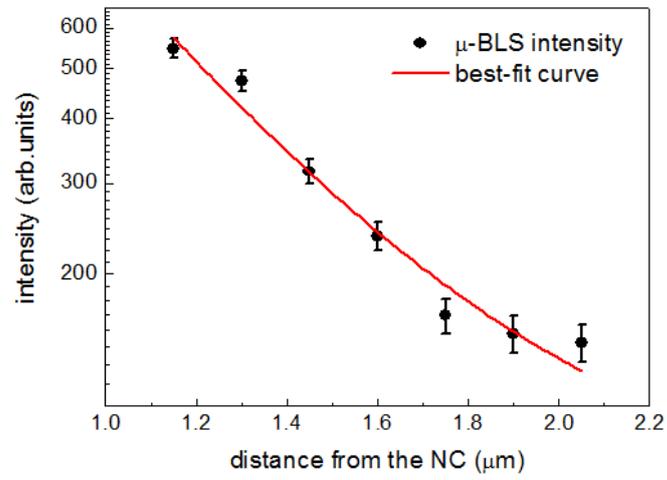
Figure 2 (color online). (circles) Spin-wave intensity measured by μ-BLS as a function of the distance (X-X_0) from the NC position. (line) Best-fit curve obtained using expression (1).
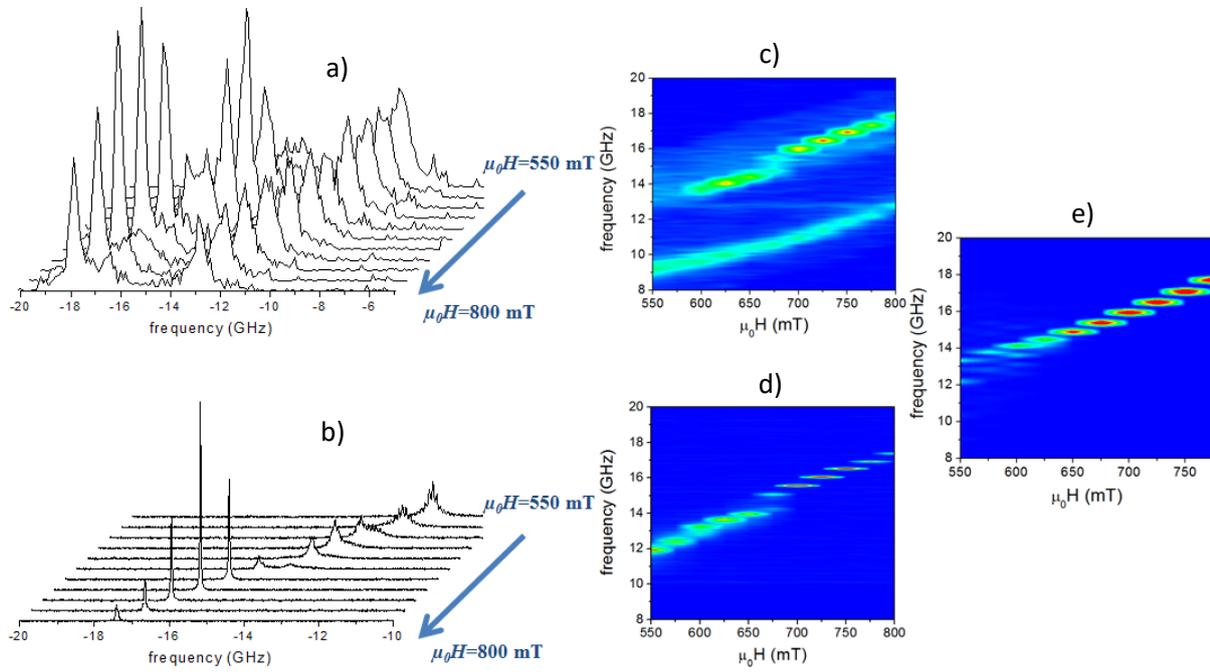
Figure 3 (color online). (a) μ-BLS and (b) SA spectra measured as a function of the intensity of the external field H for a fixed value of the injected DC $I = 30$ mA. (c) and (b) color plots of the sequence of spectra (a) and (b). (e) Results of micromagnetic simulations obtained under the same conditions.
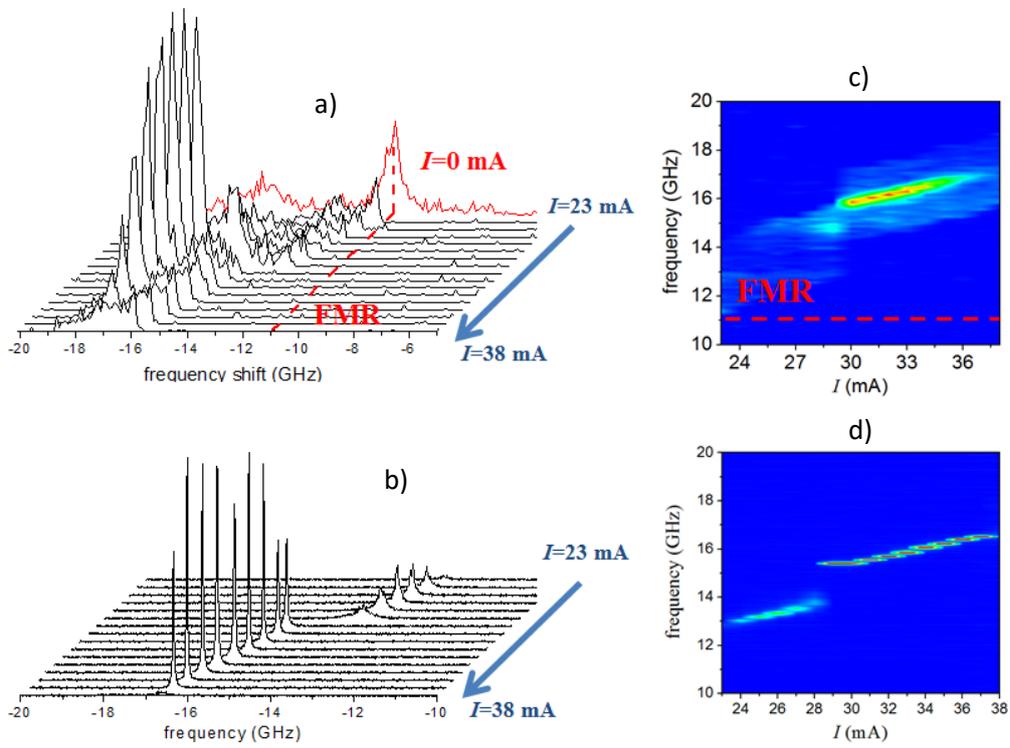
Figure 4 (color online). (a) μ-BLS and (b) SA spectra measured as a function of the intensity of the injected DC (I) for a fixed value of the external field $\boldsymbol{H}$ = 680 mT. (c) and (b) color plots of the sequence of spectra (a) and (b).
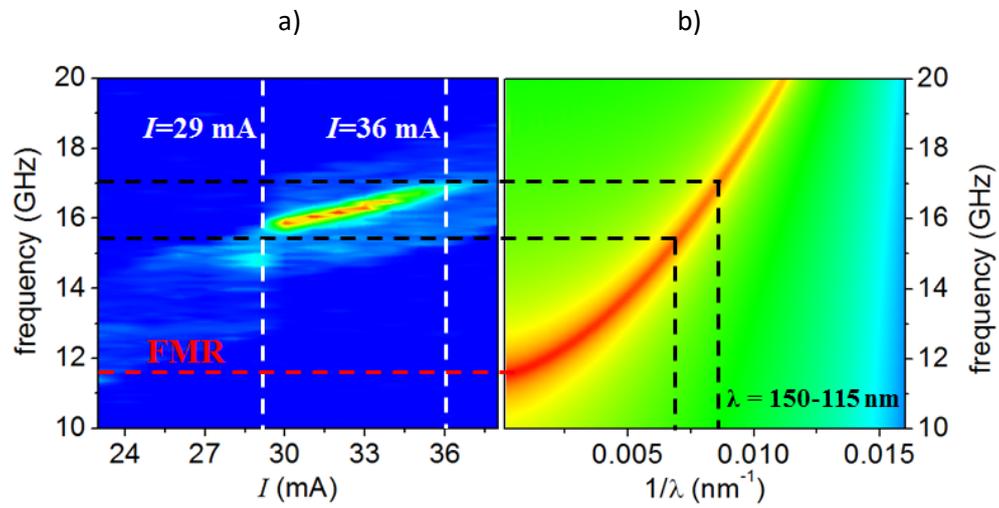
Figure 5 (color online). (a) μ-BLS spectra measured as a function of the intensity of the injected DC (I) for a fixed value of the external field $H = 680$ mT. (b) Simulated SWs dispersion curve of the NiFe free layer.
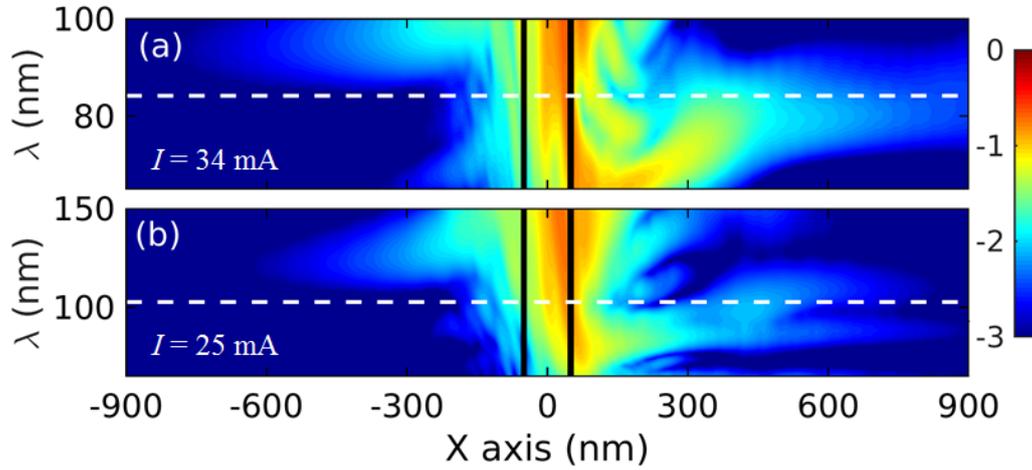
Figure 6 (color online) Smoothed pseudo-Wigner-Ville transform of simulated SWs along X for (a) $I = 34$ mA and (b) $I = 25$mA and an external field of $H = 800$ mT. The vertical black lines indicate the boundaries of the NC while the white dashed lines indicate wavelength obtained from the spin wave dispersion relation at each frequency, namely, (a) 19.2 GHz and (b) 17.1 GHz. The color contrast indicates the normalized magnitude in logarithmic scale of the SW associated with each wavelength (y axis) as a function of X.

References <mark>(TO BE UPDATED AT THE END OF ALL REVISIONS!!)</mark>

[1]   T. Silva and W. Rippard, Developments in nano-oscillators based upon spin-transfer point-contact devices, J. Magn. Magn. Mater. **320**, 1260 (2008)

[2]   R. Stamps, S. Breitkreutz, J. Åkerman, A. Chumak, Y. Otani, G. Bauer, J.-U. Thiele, M. Bowen, S. Majetich, M. Kläui, I. Prejbeanu, B. Dieny, N. Dempsey, and B. Hillebrands, The 2014 magnetism roadmap, J. Phys. D Appl. Phys. **47**, 33 (2014)

[3]   J. Åkerman, Toward a universal memory, Science **308**, 508 (2005)

[4]   J. Slonczewski, Current-driven excitation of magnetic multilayers, J. Magn. Magn. Mater. **159**, L1 (1996)

[5]   L. Berger, Emission of spin waves by a magnetic multilayer traversed by a current, Phys. Rev. B **54**, 9353 (1996)

[6]   W. Rippard, A. Deac, M. Pufall, J. Shaw, M. Keller, S. Russek, G. Bauer, and C. Serpico, Spin-transfer dynamics in spin valves with out-of-plane magnetized Co/Ni free layers, Phys. Rev. B **81**, 014426 (2010).

[7]   M.A. Hoefer, T. Silva, and M. Keller, Theory for a dissipative droplet soliton excited by a spin torque nanocontact, Phys. Rev. B. **82**, 054432 (2010)

[8]   S.M. Mohseni, S.R. Sani, J. Persson, T.N. Ahn Nguyen, S. Chung, Ye. Pogoryelov, P.K. Muduli, E. Iacocca, A. Eklund, R.K. Dumas, S. Bonetti, A. Deac, M.A. Hoefer, and J. Åkerman, Spin torque-generated magnetic droplet solitons, Science **339**, 1295 (2013)

[9]   E. Iacocca, R.K. Dumas, L. Bookman, S.M. Mohseni, S. Chung, M.A. Hoefer, and J. Åkerman, Confined dissipative droplet solitons in spin-valve nanowires with perpendicular magnetic anisotropy, Phys. Rev. Lett. **112**, 047201 (2014)

[10] F. Macià, D. Backes, and A. Kent, Stable magnetic droplet solitons in spin transfer nanocontacts, Nature Nanotechnol. **10**, 1038 (2014)

[11] M. Madami, S. Bonetti, G. Consolo, S. Tacchi, G. Carlotti, G. Gubbiotti, F. Mancoff, M. Yar, and J. Åkerman, Direct observation of a propagating spin wave induced by spin-transfer torque, Nature Nanotechnol. **6**, 635 (2011)

[12] S. Bonetti, V. Tiberkevich, G. Consolo, G. Finocchio, P.K. Muduli, F. Mancoff, A. Slavin, and J. Åkerman, Experimental evidence of self-localized and propagating spin wave modes in obliquely magnetized current-driven nanocontacts, Phys. Rev. Lett. **105**, 217204 (2010)

[13] R.K. Dumas, E. Iacocca, S. Bonetti, S.R. Sani, S.M. Mohseni, A. Eklund, J. Persson, O. Heinonen, and J. Åkerman, Spin-wave-mode coexistence on the nanoscale: a consequence of the Oersted-field-induces asymmetric energy landscape, Phys. Rev. Lett. **110**, 257202 (2013)

[14] E. Iacocca, P. Dürrenfeld, O. Heinonen, J. Åkerman, and R.K. Dumas, Mode coupling mechanisms in nanocontact spin torque oscillators, Phys. Rev. B **91**, 104405 (2015)

[15] V.E. Demidov, S. Urazhdin, and S.O. Demokritov, Direct observation and mapping of spin waves emitted by spin-torque nano-oscillators, Nature Mater. **9**, 984 (2010)

[16] T. Devolder, J.-V. Kim, M. Manfrini, W. van Roy, L. Lagae, and C. Chappert, Vortex nucleation in spin-torque nanocontact oscillators, Appl. Phys. Lett. **97**, 072512 (2010)

[17] S.R. Sani, J. Persson, S.M. Mohseni, V. Fallahi, and J. Åkerman, Current induced vortices in multi-nanocontact spin-torque devices, J. Appl. Phys. **109**, 07C913 (2011)

[18] J. Slonczewski, Excitation of spin waves by an electric current, J. Magn. Magn. Mater. **195**, 261 (1999)

[19] S. Kaka, M. Pufall, W. Rippard, T. Silva, S. Russek, and J. Katine, Mutual phase-locking of microwave spin torque nano-oscillators, Nature **437**, 389 (2005)

[20] F. Mancoff, N. Rizzo, B. Engel, and S. Tehrani, Phase-locking in double-point-contact spin-transfer devices, Nature **437**, 393 (2005)

[21] S.R. Sani, J. Persson, S.M. Mohseni, Ye. Pogoryelov, P.K. Muduli, A. Eklund, G. Malm, M. Käll, A. Dmitriev, and J. Åkerman, Mutually synchronized bottom-up multi-nanocontact spin-torque oscillators, Nature Comm. **4**, 2731 (2013)

[22] A. Houshang, E. Iacocca, P. Dürrenfeld, J. Åkerman, and R.K. Dumas, Spin wave beam mediated mutual synchronization of nano-contact spin torque oscillators, Nature Comm. *submitted* (2015)

[23] T. Kendziorczyk, S.O. Demokritov, and T. Kuhn, Spin-wave-mediated mutual synchronization o spin-torque nano-oscillators: a micromagnetic study of multistable phase locking, Phys. Rev. B **90**, 054414 (2014)

[24] F. Macià, A. Kent, and F. Hoppensteadt, Spin-wave interference patterns created by spin-torque nano-oscillators for memory and computation, Nanotechnology **22**, 095301 (2011)

[25] F. Macià, F. Hoppensteadt, and A. Kent, Spin wave excitation patterns generated by spin torque oscillators, Nanotechnology **25**, 045303 (2014)

[26] S. Bonetti and J. Åkerman, Nano-contact spin-torque oscillators as magnonic building blocks, in Magnonics, Springer. 177 (2013)

[27] S. Urazhdin, V.E. Demidov, H. Ulrichs, T. Kendziorczyk, T. Kuhn, K. Leuthold, G. Wilder, and S.O. Demokritov, Nanomagnonic devices based on the spin-transfer torque, Nature Nanotechnol. **9**, 509 (2014)

[28] M. Pufall, W. Rippard, S. Russek, S. Kaka, and J. Katine, Electrical measurement of spin-wave interaction of proximate spin transfer nanooscillators, Phys. Rev. Lett. **97**, 087206 (2006)

[29] M.A. Hoefer, T. Silva, and M. Stiles, Model for a collimated spin-wave beam generated by a single-layer spin torque nanocontact, Phys. Rev. B **77**, 144401 (2008)

[30] M. Madami, G. Gubbiotti, S. Tacchi, and G. Carlotti, Application of microfocused Brillouin light scattering to the study of spin waves in low-dimensional magnetic systems, in Solid state physics, Academic Press, 79 (2012)

[31] J. Sandercock, Light scattering in solids III, Springer Verlag, 173 (1982)

[32] M. Madami, S. Tacchi, G. Gubbiotti, G. Carlotti, F. Montoncello, G. Capuzzo, and F. Nizzoli, J. Phys. Cong. Ser. **200(4)**, 042008 (2010)

[33] A. Vansteenkiste, J. Leliaert, M. Dvornik, F. Garcia-Sanchez, and B. van Waeyenberge, The design and verification of Mumax3, **arXiv:1406.7635** (2014)

[34] M. Pufall, W. Rippard, S. Russek, and E. Evarts, Anisotropic frequency response of spin-torque oscillators with applied field polarity and direction, Phys. Rev. B **86**, 094404 (2012)